Quantification of Crystal Chemistry of Fe-Mg Carbonates by Raman Microspectroscopy and Near-Infrared Remote Sensing

Pierre Beck, Olivier Beyssac, Bernard Schmitt, Clement Royer, Lucia Mandon, Eglantine Boulard, Nicolas Rividi, Edward A Cloutis

AGU ADVANCING EARTH AND SPACE SCIENCES

Earth and Space Science

RESEARCH ARTICLE
10.1029/2024EA003666

Quantification of Crystal Chemistry of Fe-Mg Carbonates by Raman Microspectroscopy and Near-Infrared Remote Sensing

Pierre Beck[1], Olivier Beyssac[2], Bernard Schmitt[1], Clement Royer[3], Lucia Mandon[1], Eglantine Boulard[2], Nicolas Rividi[2], and Edward A. Cloutis[4]

[1]Univ. Grenoble Alpes, CNRS, IPAG, Grenoble, France, [2]Institut de Minéralogie, de Physique des Matériaux et de Cosmochimie, CNRS UMR 7590, Sorbonne Université, Muséum National d'Histoire Naturelle, Paris, France, [3]Institut d'Astrophysique Spatiale, CNRS/Paris-Saclay University, Paris, France, [4]Department of Geography, University of Winnipeg, Winnipeg, MB, Canada

Key Points:

- Fundamental FeMg carbonate mode position have a linear dependence to Mg# for Fe-Mg carbonate mineral
- Harmonic bands at 2.3 and 2.5 also have a linear dependence of their position with Mg# for Fe-Mg carbonate minerals
- We present calibration curves of Mg# versus fundamental and harmonic vibration position than can be used to retrieve crystal chemistry

Correspondence to:
P. Beck,
pierre.beck@univ-grenoble-alpes.fr

Citation:
Beck, P., Beyssac, O., Schmitt, B., Royer, C., Mandon, L., Boulard, E., et al. (2024). Quantification of crystal chemistry of Fe-Mg carbonates by Raman microspectroscopy and near-infrared remote sensing. *Earth and Space Science*, *11*, e2024EA003666. https://doi.org/10.1029/2024EA003666

Received 29 MAR 2024
Accepted 1 JUL 2024

Author Contributions:
Conceptualization: Pierre Beck, Olivier Beyssac, Bernard Schmitt
Formal analysis: Pierre Beck, Olivier Beyssac, Bernard Schmitt
Investigation: Clement Royer, Edward A. Cloutis
Methodology: Pierre Beck, Olivier Beyssac, Bernard Schmitt, Clement Royer, Lucia Mandon, Eglantine Boulard, Nicolas Rividi, Edward A. Cloutis
Writing – original draft: Pierre Beck, Olivier Beyssac, Bernard Schmitt, Clement Royer, Lucia Mandon, Eglantine Boulard, Nicolas Rividi
Writing – review & editing: Pierre Beck, Edward A. Cloutis

Abstract On Earth, carbonate minerals are widely used as recorders of the geological environments in which they formed. Here, we present a method designed to retrieve the crystal chemistry of Fe-Mg carbonate minerals using infrared remote sensing or Raman spectroscopy. We analyzed a suite of well-characterized Fe-Mg carbonate minerals for which Raman spectra were obtained in two different laboratories, and IR spectra were measured in reflectance and transmission from the visible range to 25-μm. We built calibration lines for the dependence of fundamental and harmonic vibrational modes position to the Mg# (defined as Mg# = 100 × Mg/(Mg + Fe + Ca + Mn)). These calibrations should enable retrieval of Mg# based on spectroscopic observations with a typical accuracy of 10. We discuss the framework of applicability of these calibrations and apply them to a typical CRISM spectrum of carbonates from the Nilli Fossae region of Mars.

1. Introduction

Carbonate minerals are ionic-covalent solids, in which the carbonate group (CO_3^{2-}) is associated with mono- or divalent cations (most frequently Ca^{2+}, Fe^{2+}, and Mg^{2+}). On Earth, they are generally found in sedimentary, igneous, or metamorphic rocks (Reeder, 1983; Swart, 2015). These minerals are powerful tracers of the environmental conditions in which they form, and their structure, chemistry, isotopic composition, or trace element abundances, have been used to infer their formation processes such as the chemistry of the fluid from which they precipitated. Chiefly, the presence of carbonate would generally imply alkaline fluid chemistry, and the occurrence of Fe^{2+}–rich carbonate testifies for relatively reducing conditions.

Beyond Earth, carbonate minerals have been identified throughout the Solar System. They are ubiquitous in hydrothermally altered meteorites (Brearley, 2006), and in returned samples from the CI-chondrite related asteroid Ryugu (Loizeau et al., 2023; Nakamura et al., 2022). In addition, the presence of diagnostic infrared bands has enabled their identification in remote sensing of planetary surfaces from orbit. Large carbonate veins were observed from orbit on the small near-Earth asteroid Bennu (Kaplan et al., 2020). They were also found on the dwarf planet Ceres, where Mg-rich carbonates are widespread over the surface, while Na-rich carbonates are detected in the bright material filling the Occator crater (Carrozzo et al., 2018; De Sanctis et al., 2015). In the case of comets, carbonate minerals are rare in returned samples from comet Wild-2, and may be present in comet Tempel-1 based on mid-infrared spectroscopy (Lisse et al., 2006). Beyond the Solar system, astronomical observations point toward the presence of carbonates in some stellar or protostellar environments (Ceccarelli et al., 2002), where they may form through vapor phase condensation processes (Toppani et al., 2005).

The exploration of Mars has led to the identification of carbonate minerals both in situ and from orbit, but they remain overall rare on the Martian surface. They were identified in the Nilli Fossae area based on the presence of infrared absorption bands around 2,300 and 2,500 nm, corresponding to harmonic and combination modes of the carbonate groups (Carter et al., 2023; Ehlmann et al., 2008). They were also detected based on a combination of infrared and Mossbauer spectroscopies in one outcrop at Gusev crater (Morris et al., 2010). In these two cases, the mineralogy was proposed to be in the siderite-magnesite solid solution ($FeCO_3$-$MgCO_3$). More recently, while they are generally absent in Gale crater, they were identified based on X-ray diffraction in a single outcrop (Thorpe et al., 2022). Last, they were observed in the Jezero crater at the perseverance landing site, and are again in the siderite-magnesite solid solution (Clavé et al., 2023; Scheller et al., 2022; Tice et al., 2022).

Several past studies have focused on the infrared and Raman spectroscopy of carbonates (non-exhaustively, Bishop et al., 2021; Boulard et al., 2012; Farmer, 1974; Gaffey, 1986; Rividi et al., 2010; Urmos et al., 1991). The two later papers studied the correlation between the Mg or Fe number (#) with the positions of selected Raman bands and derived linear trends over the siderite-magnesite solid solution range between the Mg# and somes peak positions. However, either the number of samples (=4) was too low (Rividi et al., 2010) or the uncertainty on the band position was too high (±2.5 cm^{-1}; Boulard et al., 2012) to determine precisely enough the correlation lines to be used in the reverse direction to accurately determine the Mg or Fe content of an unknown carbonate. In the present work, we investigate the vibrational spectra of carbonates along the siderite-magnesite solid solution, with the intent to provide tools to accurately derive the crystal chemistry of such carbonates, that is, the Fe and Mg molar fractions, based on infrared and Raman observations. This work focuses on FeMg-carbonate as such carbonate minerals are detected on Mars from orbit and from the ground (Clavé et al., 2024; Tutolo et al., 2024), but is of likely interest more generally to research focused on hydrothermal alteration of ultramafic rocks. We use some carbonate samples previously studied by Boulard et al. (2012) and Rividi et al. (2010) to record a comprehensive set of high-quality infrared and/or Raman spectra. Based on these measurements, we propose analytical formulas to derive the chemistry of the Fe-Mg carbonate based on the position of selected Raman and infrared modes, in the laboratory, in the field, or for other planetary bodies from orbit or in situ.

2. Methods

2.1. Crystal Structure and Vibrational Spectroscopy of Fe-Mg Carbonates

Magnesite ($MgCO_3$), siderite ($FeCO_3$), and calcite ($CaCO_3$) crystallize in rhombohedral symmetry within the R-3c space groups. Each cation is six-fold bonded to oxygen atoms and is associated with planar CO_3^{2-} groups (Boulard et al., 2012; Graf, 1961). Four fundamental vibrations occur in anhydrous carbonate minerals that are the ν_1 symmetric stretching, the ν_2 out-of-plane bending, the ν_3 asymmetric stretching, and finally the ν_4 in-plane bending. In the case of the siderite-magnesite structure, the ν_1 mode is not infrared active but can be probed by Raman spectroscopy while the ν_2 mode is not Raman active. In the Raman spectrum of these carbonate minerals, the ν_1 mode around 1,090 cm^{-1} is the most intense, while ν_3 and ν_4 occur respectively at about 1,440 and 715 cm^{-1}. Two translational (T) and librational (L) vibration modes are also observed around 190 cm^{-1} (T mode) and 300 cm^{-1} (L mode). The most active IR mode is the ν_3 around 1,410–1,450 cm^{-1}, followed by the ν_2 around 865–886 cm^{-1} and the ν_4 around 740–750 cm^{-1} (Figure 1).

These fundamental modes give rise to additional modes at higher wavenumber through combination and harmonics. See Bishop et al. (2021), for the most extensive survey of IR properties of carbonates at the time of writing. The first detection of carbonates on Mars from orbit was made from observations of the combination bands around 2,300 nm (interpreted as $3\nu_3$ mode), and 2,500 nm (interpreted as $2\nu_3 + \nu_1$) (Ehlmann et al., 2008). Less intense combination bands can be found at lower wavelengths (1,900, 2,000, 2,100 μm) and are usually observed only for pure carbonates. Additional combination modes occur around 3,400, 4,000, and 4,700 nm, which are significantly stronger than the 2,300 and 2,500 nm bands. These bands can be of use to identify carbonates, such as the study done for Ryugu samples with the MicrOmega spectral imager (Loizeau et al., 2023). However, this spectral range can be more challenging to measure in reflectance remote sensing, because of a lower solar flux, and to interpret due to the additional and steep contribution from thermal emission above about 3 μm in the case of surfaces of inner solar system objects.

2.2. Samples

We used eight of the samples that were characterized by Boulard et al. (2012) and provided by the Collection de Minéraux at Sorbonne Université. While their study investigated 14 samples, only 6 were available in sufficient quantity to be measured with reflectance spectroscopy. This set was completed by a few samples, including two from Rividi et al. (2010) for Raman (not IR owing to too small quantities), and one described by Chopin (1979). The crystal chemistry of these carbonates is generally CaO and MnO poor (i.e., both <1 wt.% for most, <2.5 wt.% for all but St-Georges siderite with MnO = 7.17%). The exact composition determined by Electron Microprobe Analysis is given in Table 1. The same samples were measured by near and mid-infrared spectroscopy at the Institut de Planétologie et d'Astrophysique de Grenoble (IPAG, Grenoble) and by Raman spectroscopy at Institut de Minéralogie de Physique des Matériaux et de Cosmochimie (IMPMC) in Paris and at Ecole Normale Supérieure de Lyon (ENS Lyon). When possible, samples were measured as large crystals and powder as well.

10.1029/2024EA003666

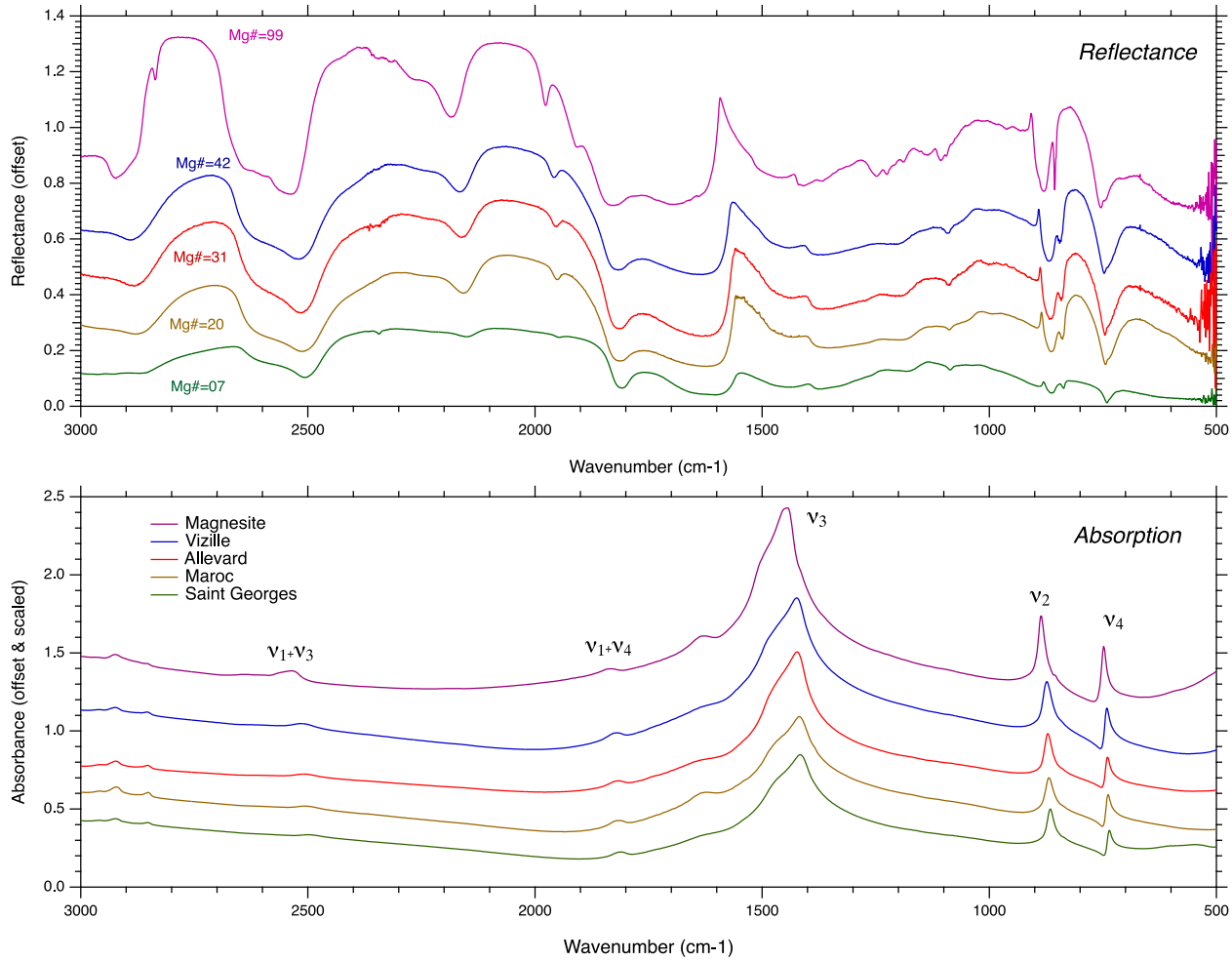

Figure 1. Fe-Mg carbonates: Mid-infrared reflectance spectra of powders (top) and transmission spectra of KBr pellets (bottom: converted to absorbance units) obtained with FTIR instruments.

2.3. IR Measurements

Infrared measurements were performed at IPAG. Reflectance spectra in the 400–4,000 nm range were recorded with the SHADOWS spectro-gonio radiometer (Potin et al., 2018). Spectra were obtained under an incidence of 0° and an emission angle of 30°, at a 10 nm spectral sampling, and a spectral resolution varying from 3 nm in the visible to 26 nm at 4 μm.

To obtain reflectance spectra at high spectral resolution, a second set of measurements in the 1.3–15.0 μm range was obtained at IPAG with a Vertex V70 Fourier-Transform IR (FTIR) spectrometer equipped with a biconical diffuse reflectance kit. They were obtained at a spectral resolution of about 1 cm^{-1}. Because remote sensing instruments may have a lower spectral resolution than what can be achieved with FTIR spectrometers in the laboratory, the FTIR reflectance spectra were also convolved and resampled at the spectral resolution of SuperCam InfraRed Spectrometer (IRS, Fouchet et al., 2022), with a spectral resolution of 32 cm^{-1} (11.4 nm at 1,950 nm).

Since the very strong fundamental bands, in the mid-IR, can be saturated in reflectance spectra and their shape altered by an interplay of the real and imaginary parts of the optical constants, the samples were also measured in transmission to determine the position of the fundamental IR active modes. For these measurements, pellets of the samples were made by diluting one mg of ground carbonate powder in 300 mg of optical-grade KBr salt. The pellets were then measured in transmission using a Bruker Vertex V70V with a 4 cm^{-1} spectral resolution.

Table 1
Chemistry, and Position of the Fundamental Vibration Modes of the Fe-Mg Carbonate Minerals Analyzed in Our Study

							Raman		Infrared (transmission)		
Sample name/origin	Source/reference	CaO wt. %	MgO wt. %	FeO wt. %	MnO wt. %	Mg # %	ν_1 (Paris) cm^{-1}	ν_1 (Lyon) cm^{-1}	ν_2 cm^{-1}	ν_3 cm^{-1}	ν_4 cm^{-1}
St-Georges (sid B)	Boulard et al. (2012)	0.83	2.47	49.1	7.17	07.1	1,085.2	1,085.6	866.01	1,415.7	736.78
Maroc	Boulard et al. (2012)	0.17	7.28	50.6	1.62	19.8	1,086.8	1,087.2	867.9	1,417.6	738.7
Jul	Boulard et al. (2012)	0.33	9.27	49.62	0.38	24.7	1,086.7	1,086.2	-	-	-
Allevard	Boulard et al. (2012)	0.43	11.62	44.81	1.60	30.6	1,087.7	1,087.9	871.8	1,423.4	740.6
Vizille	Boulard et al. (2012)	0.34	16.97	39.96	0.62	42.4	1,089.1	1,089.3	873.72	1,425.3	740.64
S2315	Boulard et al. (2012)	0.45	23.06	31.36	1.85	54.9	1,090.2	1,090.9	875.7	1,429.2	742.6
S500	Boulard et al. (2012)	0.04	29.59	25.7	0.30	66.9	1,091.8	1,092.1	879.5	1,433.0	744.5
Magnesite	Boulard et al. (2012)	0.05	47.51	0.34	0.06	99.4	1,094.4	1,094.6	885.3	1,444.6	748.3
Grainier	Rividi et al. (2010)	0.34	39.49	10.63	0.26	86.1	1,093.4	-	-	-	-
Rhodesia	Rividi et al. (2010)	2.25	45.08	0.05	0.00	96.5	1,094.6	-	-	-	-
Grand Paradis	Chopin (1979)	0.10	36	12	0.2	84.0	1,093.3	1,093.0	-	-	-

Note. The compositional data is not normalized (total < 100%), and the missing oxide is CO_2. Infrared band position were determined from transmission spectra.

Depending on the available mass of the sample, not all samples were measured with all the techniques. The required volume of sample for each measurement increases in the order Raman < KBr pellet IR < bidirectional reflectance IR < biconical reflectance IR.

2.4. Raman Measurements

All samples were analyzed using a continuous-wave Renishaw InVia Reflex Raman micro spectrometer at IMPMC in Paris. Measurements were performed using a green 532 nm solid-state laser focused on the sample through a Leica DM2500 microscope with a short working distance of 50X objective (Numerical aperture = 0.75). This configuration yields a planar resolution of approximately 1 μm^2 for a laser power delivered at the sample surface of <1 mW using neutral density filters to prevent irreversible thermal damage (Fau et al., 2019). This corresponds to a laser irradiance in the range of 0.3–1.3 10^9 $W.m^{-2}$. All measurements were performed with a circularly polarized laser using a ¼-wave plate placed before the microscope to minimize polarization effects. The Raman signal was dispersed by a grating with 2,400 lines/mm, and the signal was analyzed with a RENCAM CCD detector. Before each session, the spectrometer was calibrated in energy using a silicon standard. The spectral resolution for visible light was 1–1.9 cm^{-1}, and the wavenumber accuracy was better than 0.3 cm^{-1}. Spectra were collected using the software WIRE 4.3 provided by Renishaw.

All samples except those from Rividi et al. (2010) were also measured with the Horiba LabRAM HR800 Evolution Raman micro spectrometer of the LGLTPE laboratory at ENS-Lyon. A green 532 nm solid-state laser was also focused on the sample but through a short-working distance 100X objective. The Raman signal was dispersed by an 1,800 lines/mm grating yielding a resolution of 0.9 cm^{-1} around 1,090 cm^{-1} Raman shift. Its spectral calibration with a silicon wafer (520.7 cm^{-1}) gives a wavenumber accuracy better than 0.25 cm^{-1}. Several tests with different laser powers were made to check if it induces a modification of the shape, intensity or position of the emission bands with time (over several minutes) that may reflect either a change in chemistry of the irradiated spot or just a change in temperature, which may also induce band shift and widening. We set the final power to avoid any of those effects. Also, none of these samples displayed fluorescence with the 532 nm laser.

2.5. Determination of Peak Positions

The Raman active (ν_1) mode of the carbonate group was fitted using a pseudo-Voigt profile, after subtraction of a linear continuum. For each sample, each spectrum was fitted and the mean of the fitted peak position is given in Table 1. The position of the infrared active fundamental modes was obtained by finding the maximum absorbance in the transmission spectra of each carbonate.

In the case of reflectance spectra, three approaches were used to determine the peak position for the 2,300 and 2,500 nm bands. A first, simple approach, is to remove a linear continuum between local maxima around 2,170 and 2,600 nm, and then simply find the spectel with the lowest reflectance and use that spectel wavelength as the band position. This approach is easy to implement but its precision is limited by the spectral sampling and by the noise level.

In a second approach, we removed a linear continuum between the local maxima at about 2,170 and 2,600 nm, and the band position is obtained by fitting a third-order polynomial in the vicinity of the local minima. Typically, 5 specters on each side of the minimum were used for SHADOWS data or IRS resampled data (with a typical 10 nm spectral sampling) and 50 specters on each side of the minimum were used for FTIR reflectance spectra (with typically 0.5 nm spectral sampling).

In a third approach, we used a Multi-Gaussian Modeling (MultiGM) technique to describe the 2,300 and 2,500 nm bands. This model is based on Royer et al. (2024). In summary, a linear continuum is extracted from automatic band shoulders detection (convex upper hull method), and the continuum removed spectrum is modeled using a sum of 4 Gaussians. Thus, this representation allows for the interpolation of the band position to a better precision than the native spectral sampling (typically 1 nm in this study).

Because the 2,300 and 2,500 nm carbonate bands are asymmetric, the band minimum position depends on the spectral resolution. Therefore, to assess these effects, the different band position algorithms were run on both FTIR reflectance spectra, SHADOWS spectra, and FTIR spectra convolved to lower spectral resolution (IRS-like).

2.6. Carbonate Chemistry

In this section, we discuss the evolution of the vibrational modes as a function of crystal chemistry. The chemistry of individual carbonate minerals is taken from Boulard et al. (2012), Rividi et al. (2010), and Chopin (1979). We focus on relations between positions of IR and Raman modes with Mg#, which is taken as:

$$\text{Mg\#} = 100 \times \text{Mg}/(\text{Mg} + \text{Ca} + \text{Fe} + \text{Mn})\ \text{(molar)}$$

While Boulard et al. (2012) focused on Fe# = 100 × Fe/(Fe + Mg + Mn + Ca) we prefer here to use Mg# given the similarity in mass between Fe and Mn atoms, and the frequent replacement of Fe by Mn. Indeed, the correlations were found to be of higher quality when considering Mg# rather than Fe#. Mg# is also a classical proxy used in petrology for silicates and carbonates.

3. Results

3.1. Mid-Infrared Spectra

The infrared transmission spectra obtained on the series of Fe-Mg carbonates are shown in Figure 1 (KBr pellets, bottom panel), together with reflectance spectra obtained on powder of the same samples (Figure 1, upper panel). Because fundamental modes of the carbonate ions are particularly IR active and strong, the spectra obtained in reflectance for carbonate minerals are partly saturated below 1,700 cm^{-1}, and show a complex signature due to the interplay of the real and imaginary part of the optical constants (Figure 1, upper panel). The transmission spectra, which mostly probe the imaginary part of the optical constants are easier to interpret (Figure 1, bottom panel), and the 3 IR active fundamental modes can be observed, together with a few combination modes. Figure 2 presents zoomed views on the ν_2, ν_3, ν_4, and $\nu_1 + \nu_3$ modes for the suite of carbonate minerals we studied. These plots reveal that the position of these modes progressively shifts from low to high wavenumbers with increasing Mg#. From siderite to magnesite, the position of the ν_4 mode shifts to higher values by 11 cm^{-1}, the position of the ν_2 mode by 20 cm^{-1}, while the ν_3 mode shifts by 30 cm^{-1}. In Figure 3, the evolution of the position of each of these three modes is shown as a function of Mg#. They show a linear evolution of the position with the Mg# of the carbonates and the quality of the regression is excellent (all $R^2 > 0.985$).

3.2. Raman Spectra

A selection of representative Raman spectra measured for the suite of carbonates in Paris is shown in Figure 4. The strongest Raman mode is the ν_1 carbonate symmetric stretching mode occurring around 1,090 cm^{-1}. The ν_4

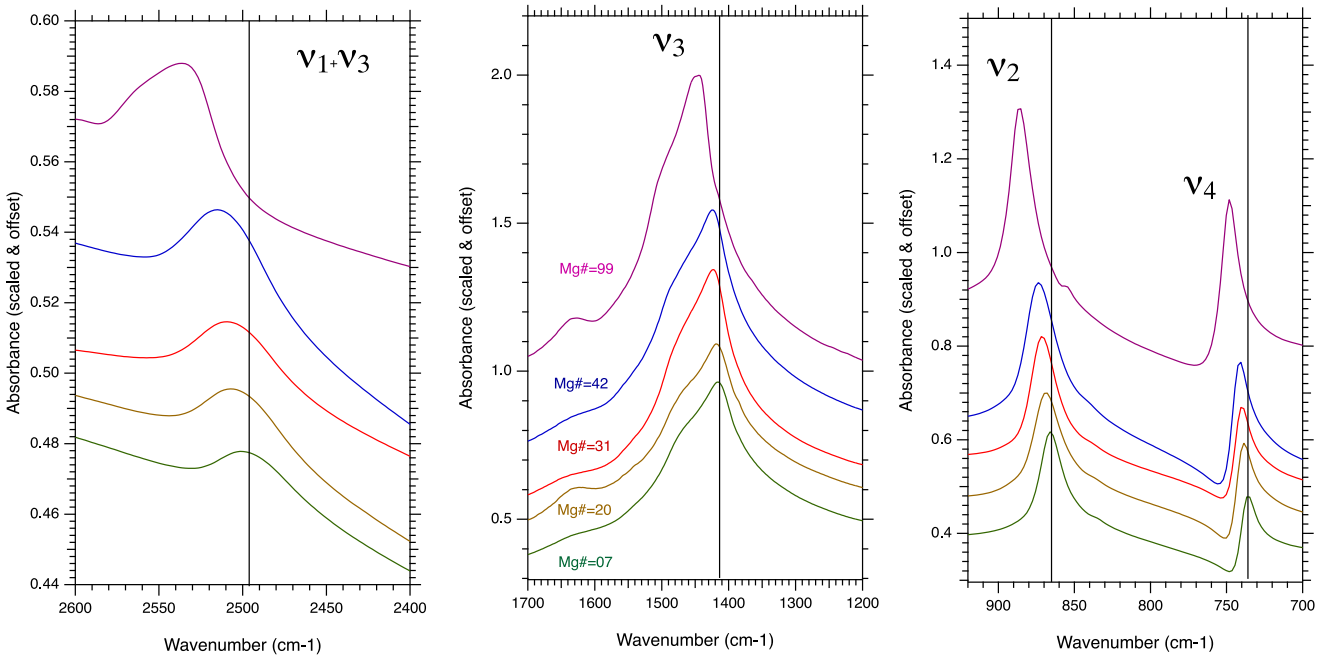

Figure 2. Closeup view on the evolution of the three IR fundamental modes and the $\upsilon_1 + \upsilon_3$ combination mode with Mg# in transmission FTIR spectra. The vertical lines give the reference position for the purest siderite (Mg# = 7%).

mode can also be observed in Figure 4, with a much lower intensity than the ν_1 mode at a position around 740 cm^{-1}. The shape of ν_4 is symmetric for magnesite but shows some level of asymmetry for some of the Fe-bearing carbonates. This asymmetry is due to the presence of a second peak forming a shoulder on ν_4 not predicted by factor group analysis, which is interpreted as infrared-only active mode becoming detectable with Raman due to the ordering of Fe atoms (Boulard et al., 2012; Langille & O'Shea, 1977). Because of this secondary mode, we did not analyze the evolution of the ν_4 mode with crystal chemistry across the siderite-magnesite solution, and focused on the most intense ν_1 vibration. This latest mode shows a linear increase of its position with Mg#, between 1,085 cm^{-1} for our most Fe-rich carbonate, toward about 1,095 cm^{-1} for the magnesite sample (Figure 5). The positions we derived based on Lorentzian fit of the ν_1 mode are in general lower than those given by Boulard et al. (2012) but they agree within their error bars (Figure 5).

3.3. Vis-NIR Reflectance Spectra and Harmonics Modes

The near-infrared reflectance spectra of 9 samples measured with the SHADOWS spectro-gonio radiometer are presented in Figure 6 in the 700–2,600 nm range, with a closeup view on the 2,200–2,600 nm spectral window. Carbonate-related absorptions are visible at 2,300 nm ($3\nu_3$) and 2,500 nm ($2\nu_3 + \nu_1$) together with smaller bands visible for some of the spectra at 1,950 and 2,150 nm. In addition, a large broad band is visible around 1,150 nm (between 700 and 1,600 nm), which is due to crystal field transitions of Fe^{2+} atoms. The band depths of all these absorptions are variable among the different samples. Note that in reflectance the band depth is not solely related to the infrared active oscillator strength, but is also related to the physical properties of the sample (grain size, porosity, presence of impurities) and cannot be used to derive chemistry of the carbonates without advanced radiative transfer modeling. The Fe^{2+} signature is very weak for the pure magnesite, but is strong for all other carbonates, without any clear correlation to Fe content.

The spectral range of the 2,300 nm and 2,500 nm bands has been measured with both SHADOWS and FTIR spectrometers. Their position was calculated for the measured FTIR data (at around 2.15–2.5 nm resolution), for these spectra interpolated at IRS spectral sampling (about 10 nm), and for the SHADOWS data (at about 20 nm resolution), using the three procedures explained in Section 2.4.

Two calibrations were built. The first one is based on our data obtained only with high spectral resolution (FTIR, in blue in Figure 7). The second one is based on data using degraded spectral resolution (10–20 nm) more akin to

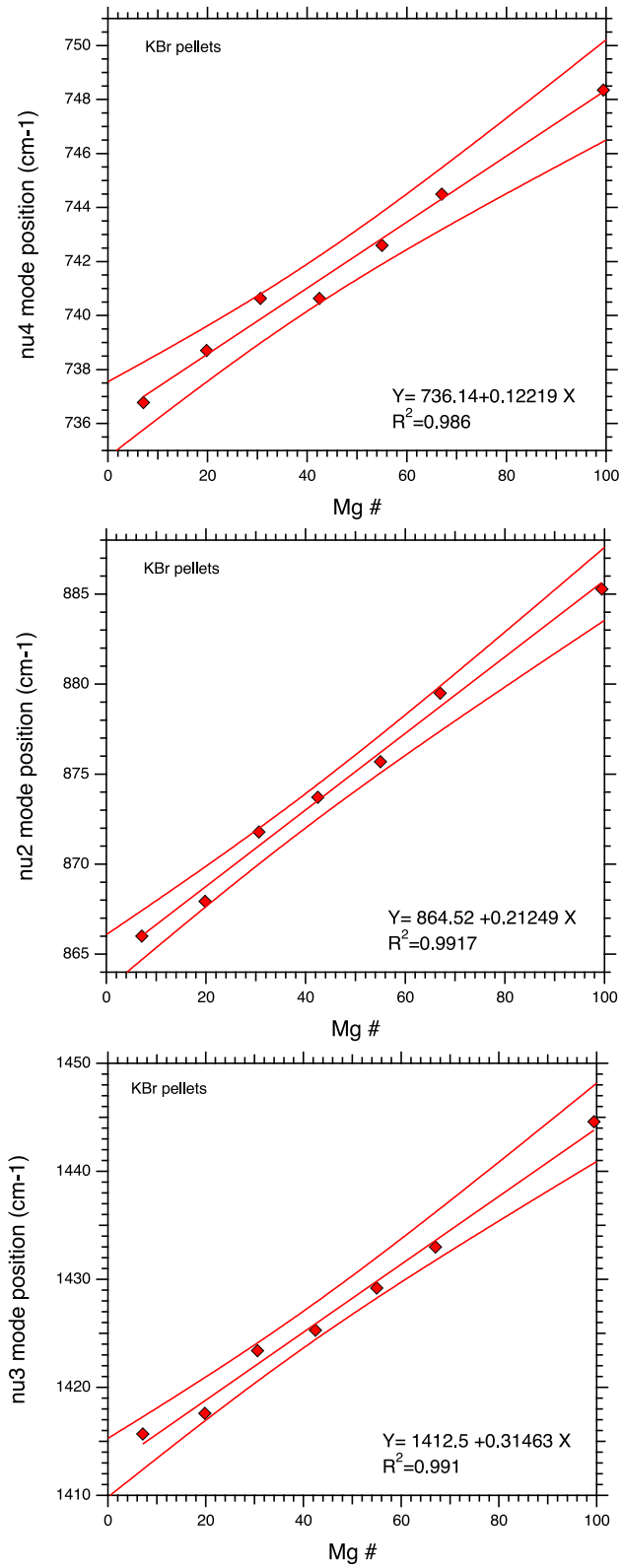

Figure 3. Evolution of the IR active fundamental carbonate modes with Mg# in Fe-Mg carbonate minerals. The red lines are linear fit to the data with 95% confidence bands.

remote sensing data. For this second calibration, we used FTIR data resampled to IRS spectral sampling, and when FTIR data were not available because of sample volume constrains, we used SHADOWS data.

They both show a monotonic decrease of the band position with increasing Mg# of the sample (from 2,330 to 2,295 and from 2,525 to 2,495 nm), with good to excellent linear correlations (R^2 from 0.841 to 0.980, Figure 7). Note that the MultiGM fit was only applied to the data at the spectral resolution of the IRS instrument (10–20 nm) since this technique was developed specifically for the M2020 SuperCam IRS instrument.

The results shown in Figure 7 reveal that the linear fit determined for the low-spectral resolution data is typically 5–10 nm lower than those measured with the FTIR spectrometer at 2.15–2.5 nm spectral resolution. This implies that accurate determination of the peak position requires careful consideration of the spectral resolution. Among all tested approaches the best correlations are found for the polynomial fits to the 2,500 nm band ($R^2 = 0.990$ and 0.978) and for the MGM fit to the 2,500 nm band ($R^2 = 0.980$).

4. Performances of the Calibration: Uncertainty, Limitations, and Case Studies

4.1. Uncertainty in the Derived Mg#

Our data set provides several ways to infer Mg# of carbonates in the siderite-magnesite solid solution using vibrational spectroscopies. The correlation laws for the different vibration modes and techniques studied are given in Table 2. The Mg# can be obtained from the relevant values of the A and B parameters:

$$\text{Mg\#} = (\text{position} - \text{A})/\text{B}$$

While the quality of the correlations is very good ($R^2 > 0.95$ for most) there are still some uncertainties on the Mg# of samples of unknown composition that can be derived based on our correlation laws. In particular, typical errors can be assessed using the confidence band (95%) shown in Figures 3 or 5.

For Raman, the determination of Mg# based on the position of the ν_1 mode has a typical accuracy between 5 and 10 if the position of the mode is known with a very high precision (<0.2 cm^{-1}). We should stress that the variations in position are small (~0.1 cm^{-1} per Mg# %) and that high-SNR and high-resolution spectra are needed for a precise determination of the crystal chemistry. An error of ±1 cm^{-1} in the peak position typically translates into an error of ±10 on the Mg#.

In the case of reflectance measurements of the 2,300 and 2,500 nm bands, the error in the determined Mg# will typically be of the order of 10. This shows that we may be able to determine the crystal chemistry of Fe-Mg carbonate with a similar uncertainty with both techniques. If both techniques are available (such as is the case for SuperCam onboard the NASA Perseverance rover, or the MicrOmega-Raman Laser Spectrometer combination onboard the ESA ExoMars rover), their combination should help reduce the error in determining Mg#. Still, the two techniques may probe different footprints and depths within the samples, since the optical path length in the visible (where Raman scattering is excited) may be different from the optical path length in the infrared where carbonate bands occur.

10.1029/2024EA003666

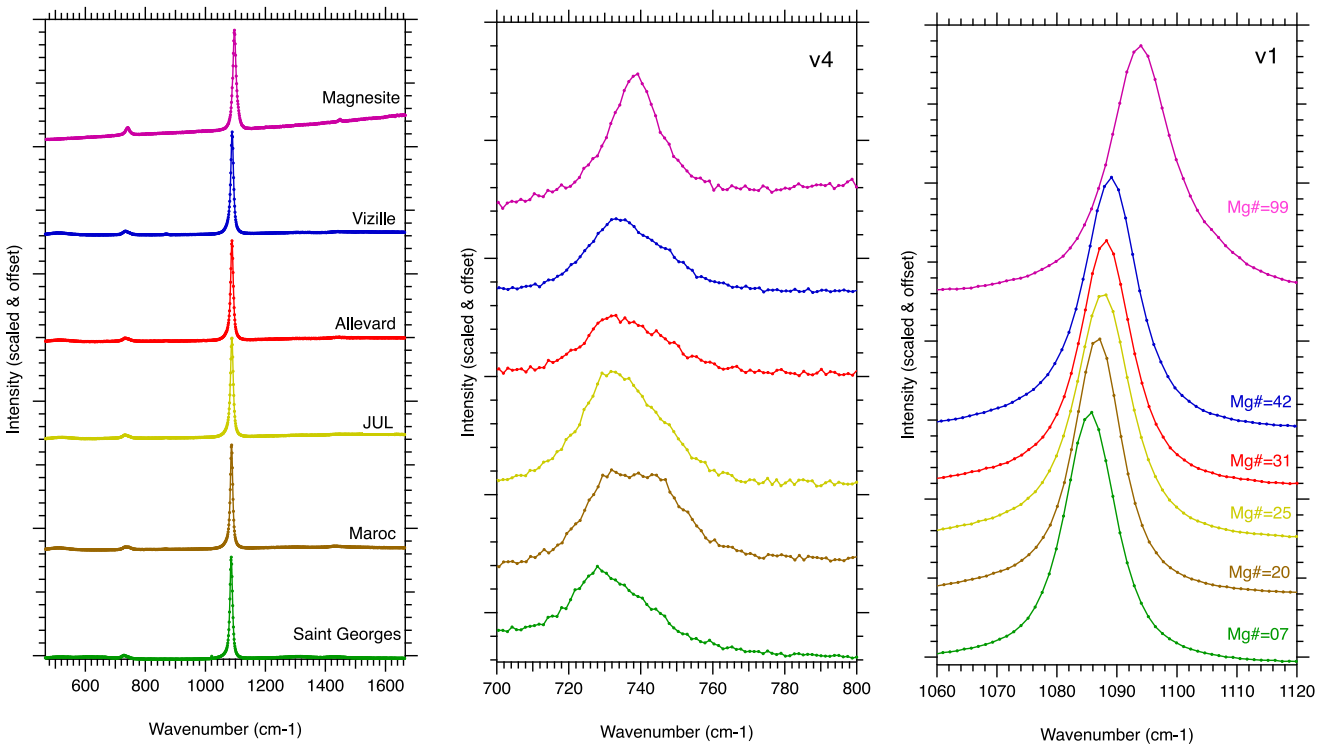

Figure 4. Evolution of the Raman active carbonate modes with Mg# in Fe-Mg carbonate minerals. Left: full spectra, center: υ_4 mode, right: υ_1 mode.

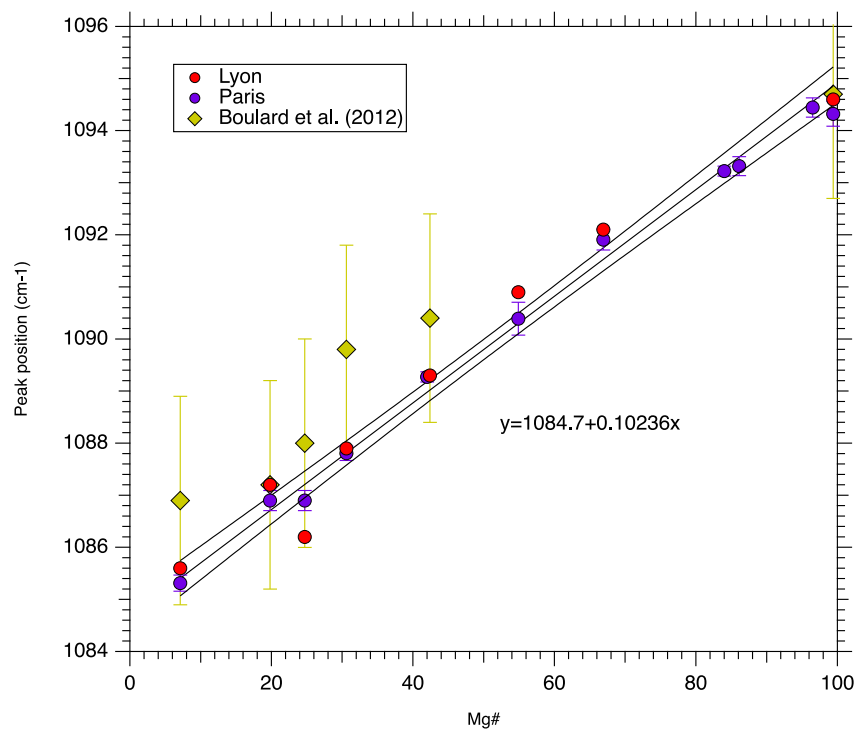

Figure 5. Position of the ν_1 mode with Mg# determined from Raman measurements from this study (from ENS Lyon and IMPMC Paris) compared to Boulard et al. (2012). The black line is a fit to ENS Lyon and IMPMC Paris data with 95% confidence bands.

10.1029/2024EA003666

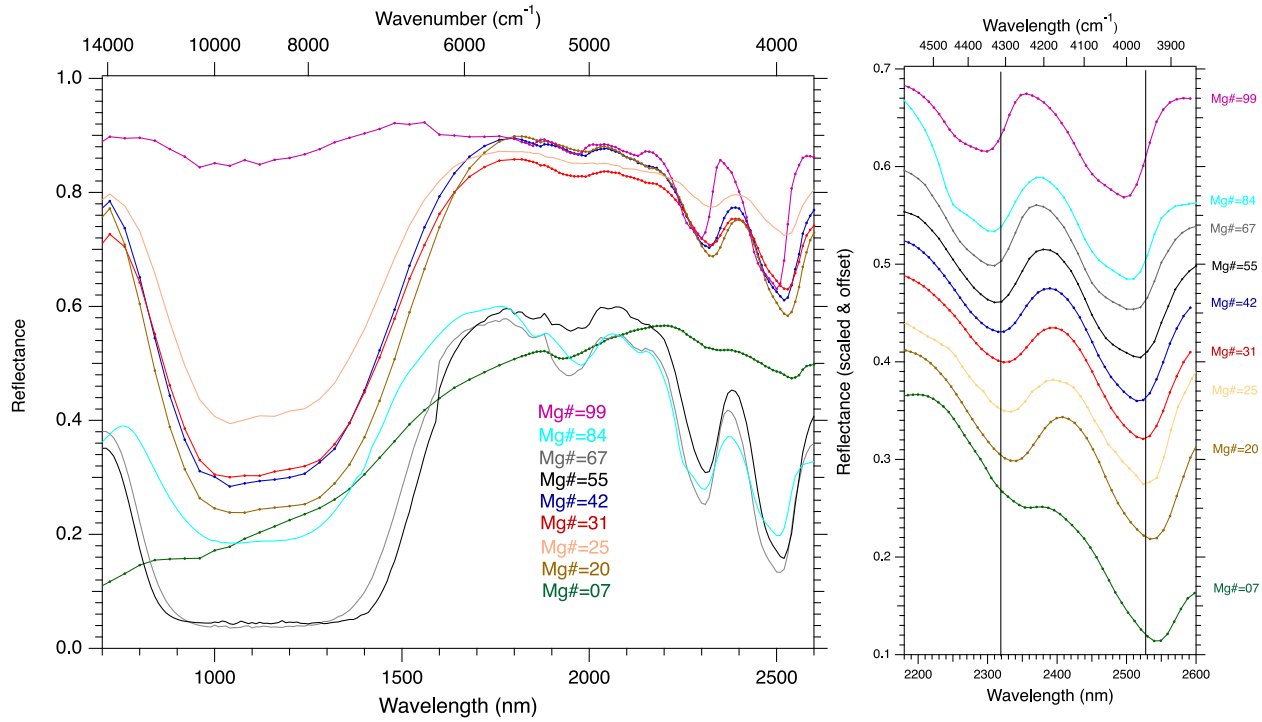

Figure 6. Near infrared reflectance spectra of FeMg carbonates measured with the SHADOWS spectro-gonio radiometer. The right panel is a focus on the 2,300 nm and 2,500 nm bands where spectra are scaled and offset. The vertical lines give the reference positions for the purest siderite (Mg# = 7%).

4.2. Attribution of the 2,300 and 2,500 nm Bands

Since we measured both fundamental and harmonic vibration modes, we can verify the attributions of the 2,300 and 2,500 nm bands. In particular, the transmission mid-IR spectra we measured enable to remove most of the uncertainty related to particle size effects when assessing the position of fundamental modes from reflectance spectra. The position of the fundamental modes we derived is given in Table 3. The accuracy of these positions is reinforced by verifying the position of the simplest combinations for magnesite, that is, $\nu_1 + \nu_2$ measured at 1,976 cm^{-1} (while estimated at 1,980 cm^{-1} from the simple sum of the fundamental modes), $\nu_3 + \nu_4$ measured at 2,185 cm^{-1} (estimated at 2,193 cm^{-1}) and last $\nu_1 + \nu_3$ measured at 2,536 cm^{-1} (estimated at 2,540 cm^{-1}).

While there was initially some debate on whether these modes could be due to combinations of the $2\nu_3$ mode with lattice vibrations (Hexter, 1958), the 2,300 and 2,500 nm bands are generally attributed to $3\nu_3$ and $2\nu_3 + \nu_1$ respectively (see for instance Gunasekaran et al., 2006). However, it was shown by Bishop et al. (2021) that several combination modes should be present in the vicinity of these two bands and could contribute.

In the case of the 2,300 nm band (measured at 4,346 cm^{-1} for magnesite, see also table 3), we found four possible combination modes that may contribute: the $3\nu_3$ (calculated at 4,334 cm^{-1}), $2\nu_1 + \nu_3 + \nu_4$ (4,383 cm^{-1}) and last, the $2\nu_3 + 2\nu_4$ (4,386 cm^{-1}). These calculations are simply the corresponding sums of the fundamental frequencies and did not take into account anharmonicity and mode interactions that systematically shift the effective position of the combination and overtone modes to lower wavenumber. The $3\nu_3$ may be a major contributor to this band since its fundamental vibration is the most IR active and it has only three quanta. While the calculation of $3\nu_3$ based on the position of the most intense component of ν_3 is unexpectedly lower than that measured (4,346 cm^{-1} measured vs. 4,334 cm^{-1} estimated), the use of the $2\nu_3$ (measured at 2,926 cm^{-1}) to estimate the position of $3\nu_3$ yields to a better agreement (i.e., the prediction is at higher wavenumber than the observation, 4,346 cm^{-1} measured vs. 4,386 cm^{-1} estimated). A probable reason is that it is the weakest ν_3 component (present in the form of a shoulder of the main peak) that creates the peak intensity of the harmonic modes. It is possible that the $2\nu_1 + \nu_3 + \nu_4$ or $2\nu_3 + 2\nu_4$ modes, despite having more quanta than $3\nu_3$ and thus most probably lower intensity, contribute to creating the band (Table 3) and may explain the asymmetry of the whole 2,300 nm band.

10.1029/2024EA003666

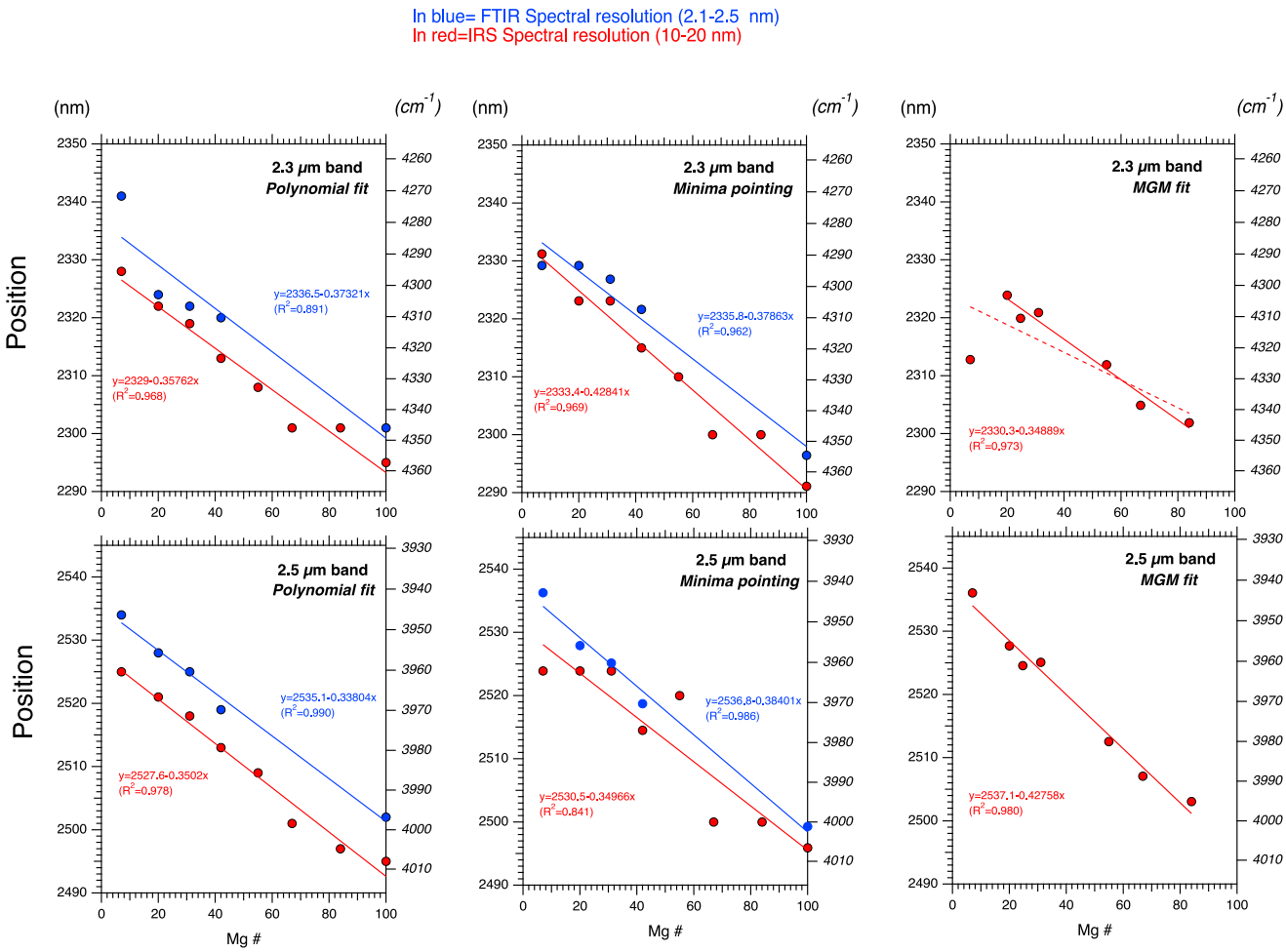

Figure 7. Evolution of the 2,300 and 2,500 nm band positions determined with three approaches (polynomial fit, minima pointing and MGM fit). The red dots are the positions determined from data at 10–20 nm spectral resolution (IRS resampled or SHADOWS data) while the blue points are positions determined from FTIR spectra (<2.5 nm spectral resolution). The red and blue lines are linear fits to the data. See text for details.

In the case of the 2,500 nm bands (measured at 3,997 cm^{-1} for magnesite, see also table 3), we found two possible combination modes that are $\nu_1 + 2\nu_3$ (estimated at 3,983 cm^{-1}) and $\nu_1 + \nu_3 + 2\nu_4$ (4,035 cm^{-1}). The estimation of the $\nu_1 + 2\nu_3$ mode position based on ν_1 and the peak position of ν_3 is at 3,983 cm^{-1}, thus lower than the measured value (3,997 cm^{-1}). However, when the estimate is made from the measured $2\nu_3$ and ν_1 positions, the value becomes consistent, at 4,021 cm^{-1}. The $\nu_1 + \nu_3 + 2\nu_4$ is calculated at 4,035 cm^{-1} and may additionally contribute to the low-frequency wing.

The same reasoning can also be done for siderite, leading to the same conclusion as all the bands are systematically shifted to lower frequency.

4.3. Remote Determination of Carbonate Chemistry From Raman Data

We test here the capability of our approach to simulate Raman spectra of the Martian surface recorded by the SuperCam instrument (see Maurice et al., 2021; Wiens et al., 2021 for the instrument capabilities). We produced a synthetic Lorentzian peak with a FWHM of 12 cm^{-1}, sampled at 2 cm^{-1}, similar to the υ_1 main carbonate band that should be recorded by the Raman part of the SuperCam instrument suite. A white noise was added to the spectra to simulate data of variable quality, that may be obtained for different accumulation numbers of laser shots with this time-resolved instrument using a pulsed laser. Multiple tests were run where different levels of white noise were added to a Lorentzian shape peak to simulate different values of SNR. The peak position was then

Table 2
Linear Fit Parameters Obtained From the Analysis of Band Position of Various Vibration Modes as a Function of Mg#

Mode/Band Position = A + B × Mg#	A coeff.	B coeff.	R^2
IR			
ν_2	864.52 ± 1.21	0.21249 ± 0.0223	0.992
ν_3	1,412.5 ± 1.91	0.31463 ± 0.0353	0.991
ν_4	736.14 ± 0.90	0.12219 ± 0.0167	0.986
2.3 μm polynomial fit			
high spectral resolution	2,336.5 ± 12.3	−0.37321 ± 0.24	0.891
IRS-like spectral resolution	2,329.0 ± 3.8	−0.35762 ± 0.0645	0.968
2.3 μm minima pointing			
high spectral resolution	2,335.8 ± 7.13	−0.37863 ± 0.14	0.962
IRS-like spectral resolution	2,333.4 ± 4.5	−0.42841 ± 0.0764	0.969
2.5 μm polynomial fit			
high spectral resolution	2,535.1 ± 3.2	−0.32675 ± 0.0208	0.990
IRS-like spectral resolution	2,527.6 ± 3.06	−0.33804 ± 0.0624	0.978
2.5 μm minima pointing			
high spectral resolution	2,536.8 ± 4.3	−0.37401 ± 0.0838	0.986
IRS-like spectral resolution	2,530.5 ± 8.94	−0.34966 ± 0.15	0.841
Raman			
ν_1	1,084.7 ± 0.377	0.10236 ± 0.00638	0.994

Note. See text for details.

determined by fitting the synthetic spectra in the same way as done for the laboratory measurements presented here.

Results (Figure 8) show that for SNR above 100 (SNR is defined as the ratio between the mean and standard deviation of the signal, in other words the amplitude of the peak divided by the square root of the variance of the white noise), the position of the peak may be determined with an accuracy better than 0.1 cm^{-1}, leading to an 1-σ error on Mg# of ±1. For an SNR of 10, the error becomes around 0.5 cm^{-1} causing an error in Mg# of ±5. In the worst case we investigated, a SNR of 2, the error on the position was about ±3 cm^{-1}, leading to an error of ±30 on Mg#. To this error, the uncertainty on the absolute calibration should be added, as well as the uncertainty on the Raman mode position versus Mg calibration.

While the exact performances of SuperCam Raman are still being evaluated, this analysis shows that it may be able to retrieve carbonate chemistry with an accuracy similar to that of VISIR spectroscopy.

4.4. Limitations, and Framework of Applicability

We should stress that the calibration we developed is based on pure phase analysis. In any natural samples or when observing a natural surface, or a geological outcrop, carbonates will likely be mixed with other minerals or organic phases or dust.

In the case of Raman spectroscopy, measurements are performed at the micron scale on single crystals. Each crystal is measured on a few spots to assess its homogeneity. However even in case of mixture with another compound may decrease the Raman signal, but should not impact the band position.

In the case of infrared spectroscopy, if the carbonates are mixed with FeMg-phyllosilicates, the position of the 2,300 nm carbonate harmonic mode will be impacted by the superimposed metal-OH absorption from phyllosilicates. In that case, the use of the 2,500 nm band is preferred for inferring carbonate crystal chemistry, and its use should still be reliable. One exception is if carbonates are mixed with serpentines that can have overlapping absorptions both on the 2,300 and 2,500 nm bands. Mixtures with anhydrous silicates should not impact the

Earth and Space Science

10.1029/2024EA003666

Table 3

Position of the Fundamental Vibrational Modes of the Carbonate Group in Siderite (Mg# = 7) and Magnesite (Mg# = 100), and Estimations of the Positions of Overtone and Combination Bands for the 2,300 and 2,500 nm Bands Using the υ_1, υ_2, υ_4 Fundamentals and the $2\upsilon_3$ Overtone

	Fundamental						Combination									
	Measured						Measured	Measured	Estimation				Measured	Estimation		
	ν_1 Raman cm^{-1}	ν_2 IR cm^{-1}	ν_3 IR cm^{-1}	ν_3 Raman cm^{-1}	ν_4 IR cm^{-1}	ν_4 Raman cm^{-1}	$2\nu_3$ IR cm^{-1}	2,300 nm band IR cm^{-1}	$3\nu_3$ cm^{-1}	$3\nu_3$[a] cm^{-1}	$2\nu_3 + 2\nu_4$ cm^{-1}	$2\nu_1 + \nu_3 + \nu_4$ cm^{-1}	2,500 nm band IR cm^{-1}	$\nu_1 + 2\nu_3$ cm^{-1}	$\nu_1 + 2\nu_3$[a] cm^{-1}	$\nu_1 + \nu_3 + 2\nu_4$ cm^{-1}
siderite	1,085	866	1,416	1,431	737	728	2,861	4,280	4,247	4,303	4,306	4,323	3,945	3,917	3,946	3,975
magnesite	1,095	885	1,445	1,446	748	739	2,926	4,346	4,334	4,386	4,386	4,383	3,997	3,983	4,021	4,035

[a]Position based on measured position of $2\nu_3$.

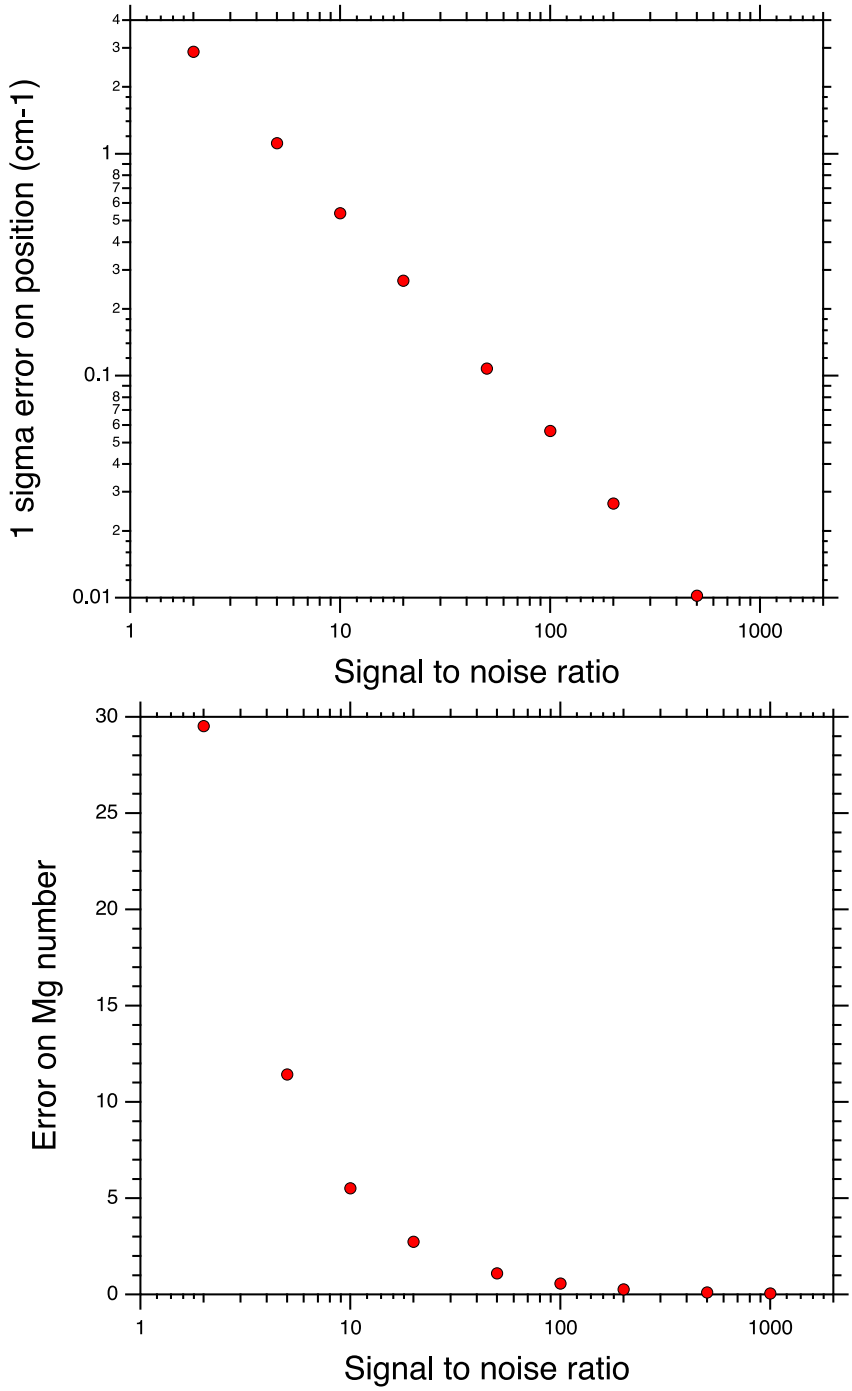

Figure 8. Error model for determination of the υ_1 band position and carbonate mineral crystal chemistry (Mg#) from simulated Raman spectra.

determination of band positions and retrieval of carbonate composition. Last, the presence of hydrated silica or Al-rich clays mixed with carbonate may introduce a wing on the 2.3 μm band, making the detection of its position more challenging. In that case, again, the use of the position of the 2.5 μm band for determining carbonate crystal chemistry is preferred.

The calibrations presented here are designed for carbonates in the magnesite-siderite solid solutions and then do not apply to other types of carbonates bearing Ca or Mn for instance. In planetary remote sensing, we may need

complementary information on the nature of the carbonate phase to make sure it is applicable. The positions of the 2,300 nm, 2,500 nm, and the ν_1 mode for pure magnesite are not ambiguous (i.e., characteristic of magnesite), but these positions can be similar between the Fe-rich endmembers of the Fe-Mg solid solution with pure Ca carbonates (calcite or aragonite) or dolomite. Calcite should be easily identified from its generally high reflectance and lack of Fe^{2+} absorption, but Fe-dolomite ankerite-type carbonates may be more challenging to identify based only on the reflectance spectra or position of ν_1 Raman mode as both of them are similar to Fe-rich magnesite. Raman is also limited for discriminating pure Fe-Mg carbonates from Fe-Mg carbonates including Ca and/or Mn. Contribution of Ca and/or Mn may be challenging to assess but the other modes may be used if they are measured with enough accuracy (Rividi et al., 2010). Only Fe-poor dolomite can be discriminated with its higher ν_1 vibration frequency, up to 1,099 cm^{-1}. In the case of Raman spectra, the other weaker modes may be used if they are measured with enough accuracy. In the case of infrared spectra up to 2,600 nm, we may combine optical remote sensing with chemical analysis, such as LIBS or X-ray fluorescence, to assess whether the sample contains a significant amount of Ca.

Last, this calibration was built for anhydrous FeMg carbonates and is not applicable so far as we can tell to hydrated FeMg carbonates. In the case of infrared, hydrated carbonates should be recognizable from the absorption related to water at 1.9 μm. Similarly, in Raman, the search for water signature around 3,400 cm^{-1} (OH stretch in H_2O) or 3,600–3,700 (OH stretch in OH radical) will help exclude (or recognize) the presence of a hydrated carbonate.

4.5. Application of the VNIR Calibration to CRISM Data on Nilli Fossae Carbonate

To test the applicability of the method to infrared remote sensing data we used observation of carbonates from the CRISM spectral library (Ehlmann et al., 2008; Viviano-Beck et al., 2014). We used a ratioed spectrum, intended to maximize carbonate signatures, that was taken within the Nilli Fossae area (https://crismtypespectra.rsl.wustl.edu/; source image = FRT00003E12_07_IF166J_TER3; spectrum position = (136,103), position of reference spectrum = (136, 211), size of ROI = 5 × 5). Using the procedure described above, we analyzed the position of the two carbonate bands and found that the location of the maxima of absorption are at 2,304.6 and 2,503.1 nm. If we make the strong hypothesis that these carbonates are in the Fe-Mg solid solution, these band positions can be converted into Mg# based on table 1, which provides values of 68.2 ± 6 and 72.5 ± 5 for the 2,300 and 2,500 nm bands respectively using the polynomial IRS-like spectral calibration.

These two values are in good agreement with each other and suggest that the carbonate present in the Nilli Fossae area is not pure magnesite but contains some fraction of iron. These values are close to the Mg# proposed for the Martian mantle (67–80; Anderson, 1972; Sanloup et al., 1999; Wänke & Dreibus, 1988; Yoshizaki & McDonough, 2020), and may suggest a formation process through the isochemical alteration of mantellic olivine, although several other scenarios could be proposed.

5. Conclusions

We provide in this paper an analysis of the vibrational spectra of Fe-Mg carbonate minerals. Samples were measured with Raman spectroscopy, as well as infrared reflectance and transmission spectroscopy.

This work sheds new light on the dependence of the various CO_3-related modes with crystal chemistry. All analyzed absorptions (fundamental modes, 2,300 nm, and 2,500 nm bands) reveal a linear behavior with Mg# (defined as 100 × Mg/(Mg + Ca + Fe + Mn)).

We provide in Table 2 a calibration of the dependence of these absorptions which should enable the determination of carbonate crystal chemistry from analysis of the band position. These calibrations should typically enable retrieval of Mg# with an accuracy of about ±5 from a Raman spectrum with a SNR above 500. For IR fundamental modes the calibration accuracy is a bit worse, with an error that should be below typically ±10.

Given the asymmetry of the 2,300 nm and 2,500 nm bands, their positions depend on the spectral resolution of the measurements. We thus provide calibrations for typical high-resolution FTIR spectra, as well as lower-resolution spectra. We also analyzed the origin of these two bands, by estimating the position of combination modes of the fundamental modes that we measured. These calculations are in agreement with previous attributions that the 2,300 nm band is related to $3\nu_3$ (with a possible contribution from $2\nu_1 + \nu_3 + \nu_4$ or $2\nu_3 + 2\nu_4$) and that the 2,500 nm band is related to $\nu_1 + 2\nu_3$ (with a possible contribution from $\nu_1 + \nu_3 + 2\nu_4$).

Finally, we assessed the requirement in terms of SNR to retrieve accurate chemistry with Raman remote sensing and applied the calibration of the 2,300 nm and 2,500 nm band positions to a CRISM type spectrum of carbonate from the Nili Fossae area, under the hypothesis that these carbonates are purely Fe-Mg.

Data Availability Statement

The complete sets of spectral data (Beck et al., 2023) presented in this paper are available online in the DRIMS database of the SSHADE database infrastructure (https://vwww.sshade.eu): https://doi.org/10.26302/SSHADE/EXPERIMENT_BS_20240605_001.

Acknowledgments
The authors warmly thank Christian Chopin (ENS Paris) for providing the Grand Paradis sample. Funding from the Centre National d'Etude Spatiale (CNES) in the framework of M2020, MSL and MMX support is also acknowledged. We also thank the Collection de Minéraux at Sorbonne Université for the loan of carbonate samples and the Raman micro-spectroscopy platform in ENS Lyon supported by CNRS–INSU. The authors sincerely acknowledge precious comments from Janice Bishop and an anonymous reviewer.

References

Anderson, D. L. (1972). Internal constitution of Mars. *Journal of Geophysical Research*, *77*(5), 789–795. https://doi.org/10.1029/jb077i005p00789

Beck, P., Beyssac, O., & Schmitt, B. (2023). Near and Mid-IR reflectance, Mid-IR transmission and Raman emission spectra of a series of Fe-Mg carbonates along the Siderite-Magnesite solid solution. SSHADE/GhoSST+DRIMS (OSUG Data Center). *Dataset/Spectral Data*. https://doi.org/10.26302/SSHADE/EXPERIMENT_BS_20240605_001

Bishop, J. L., King, S. J., Lane, M. D., Brown, A. J., Lafuente, B., Hiroi, T., et al. (2021). Spectral properties of anhydrous carbonates and nitrates. *Earth and Space Science*, *8*(10), e01844. https://doi.org/10.1029/2021EA001844

Boulard, E., Guyot, F., & Fiquet, G. (2012). The influence on Fe content on Raman spectra and unit cell parameters of magnesite-siderite solid solutions. *Physics and Chemistry of Minerals*, *39*(3), 239–246. https://doi.org/10.1007/s00269-011-0479-3

Brearley, A. J. (2006). The action of water. In *Meteorites and the early solar system* (pp. 587–624).

Carrozzo, F. G., De Sanctis, M. C., Raponi, A., Ammannito, E., Castillo-Rogez, J., Ehlmann, B. L., et al. (2018). Distribution of carbonates on ceres. In *49th annual lunar and planetary science conference* (p. 2336).

Carter, J., Riu, L., Poulet, F., Bibring, J.-P., Langevin, Y., & Gondet, B. (2023). A Mars orbital catalog of aqueous alteration signatures (MOCAAS). *Icarus*, *389*, 115164. https://doi.org/10.1016/j.icarus.2022.115164

Ceccarelli, C., Caux, E., Tielens, A. G. G. M., Kemper, F., Waters, L. B. F. M., & Phillips, T. (2002). Discovery of calcite in the solar type protostar NGC 1333-IRAS 4. *Astronomy and Astrophysics*, *395*(2), L29–L33. https://doi.org/10.1051/0004-6361:20021490

Chopin, C. (1979). De la Vanoise au Massif du Grand Paradis: une approche pétrographique et radiochronologique de la signification géodynamique du métamorphisme de haute pression.

Clavé, E., Beck, P., Dehouck, E., Forni, O., Schröder, S., Mangold, N., et al. (2024). Diversity of carbonates in Jezero Crater, Mars, as seen with the SuperCam instrument. In *LPI contributions* (p. 1829).

Clavé, E., Benzerara, K., Meslin, P.-Y., Forni, O., Royer, C., Mandon, L., et al. (2023). Carbonate detection with SuperCam in igneous rocks on the floor of Jezero Crater, Mars. *Journal of Geophysical Research: Planets*, *128*(6), e2022JE007463. https://doi.org/10.1029/2022JE007463

De Sanctis, M. C., Ammannito, E., Raponi, A., Marchi, S., McCord, T. B., McSween, H. Y., et al. (2015). Ammoniated phyllosilicates with a likely outer Solar System origin on (1) Ceres. *Nature*, *528*(7581), 241–244. https://doi.org/10.1038/nature16172

Ehlmann, B. L., Mustard, J. F., Murchie, S. L., Poulet, F., Bishop, J. L., Brown, A. J., et al. (2008). Orbital identification of carbonate-bearing rocks on Mars. *Science*, *322*(5909), 1828–1832. https://doi.org/10.1126/science.1164759

Farmer, V. C. (1974). Infrared spectra of minerals. *Mineralogical Society*.

Fau, A., Beyssac, O., Gauthier, M., Meslin, P. Y., Cousin, A., Benzerara, K., et al. (2019). Pulsed laser-induced heating of mineral phases: Implications for laser-induced breakdown spectroscopy combined with Raman spectroscopy. *Spectrochimica Acta - Part B: Atomic Spectroscopy*, *160*, 105687. https://doi.org/10.1016/j.sab.2019.105687

Fouchet, T., Reess, J.-M., Montmessin, F., Hassen-Khodja, R., Nguyen-Tuong, N., Humeau, O., et al. (2022). The SuperCam infrared spectrometer for the perseverance rover of the Mars2020 mission. *Icarus*, *373*, 114773. https://doi.org/10.1016/j.icarus.2021.114773

Gaffey, S. J. (1986). Spectral reflectance of carbonate minerals in the visible and near infrared (0.35-2.55 microns); calcite, aragonite, and dolomite. *American Mineralogist*, *71*, 151–162.

Graf, D. L. (1961). Crystallographic tables for the rhombohedral carbonates. *American Mineralogist*, *46*, 1283–1316.

Gunasekaran, S., Anbalagan, G., & Pandi, S. (2006). Raman and infrared spectra of carbonates of calcite structure. *Journal of Raman Spectroscopy*, *37*(9), 892–899. https://doi.org/10.1002/jrs.1518

Hexter, R. M. (1958). High-resolution, temperature-dependent spectra of calcite. *Spectrochimica Acta*, *10*(3), 281–290. https://doi.org/10.1016/0371-1951(58)80094-6

Kaplan, H. H., Lauretta, D. S., Simon, A. A., Hamilton, V. E., DellaGiustina, D. N., Golish, D. R., et al. (2020). Bright carbonate veins on asteroid (101955) Bennu: Implications for aqueous alteration history. *Science*, *370*(6517). https://doi.org/10.1126/science.abc3557

Langille, D. B., & O'Shea, D. C. (1977). Raman spectroscopy studies of antiferromagnetic $FeCO_3$ and related carbonates. *Journal of Physics and Chemistry of Solids*, *38*(10), 1161–1171. https://doi.org/10.1016/0022-3697(77)90044-0

Lisse, C. M., VanCleve, J., Adams, A. C., A'Hearn, M. F., Fernandez, Y. R., Farnham, T. L., et al. (2006). Spitzer spectral observations of the deep impact ejecta. *Science*, *313*(5787), 635–640. https://doi.org/10.1126/science.1124694

Loizeau, D., Pilorget, C., Riu, L., Brunetto, R., Bibring, J.-P., Nakato, A., et al. (2023). Constraints on solar system early evolution by MicrOmega analysis of Ryugu carbonates. *Nature Astronomy*, *7*(4), 391–397. https://doi.org/10.1038/s41550-022-01870-1

Maurice, S., Wiens, R. C., Bernardi, P., Caïs, P., Robinson, S., Nelson, T., et al. (2021). The SuperCam instrument suite on the Mars 2020 rover: Science objectives and mast-unit description. *Space Science Reviews*, *217*(3), 47. https://doi.org/10.1007/s11214-021-00807-w

Morris, R. V., Ruff, S. W., Gellert, R., Ming, D. W., Arvidson, R. E., Clark, B. C., et al. (2010). Identification of carbonate-rich outcrops on Mars by the spirit rover. *Science*, *329*(5990), 421–424. https://doi.org/10.1126/science.1189667

Nakamura, T., Matsumoto, M., Amano, K., Enokido, Y., Zolensky, M. E., Mikouchi, T., et al. (2022). Formation and evolution of carbonaceous asteroid Ryugu: Direct evidence from returned samples. *Science*, *0*(6634), eabn8671. https://doi.org/10.1126/science.abn8671

Potin, S., Brissaud, O., Beck, P., Schmitt, B., Magnard, Y., Correia, J.-J., et al. (2018). SHADOWS: A spectro-gonio radiometer for bidirectional reflectance studies of dark meteorites and terrestrial analogs: Design, calibrations, and performances on challenging surfaces. *Applied Optics*, *57*(28), 8279–8296. https://doi.org/10.1364/AO.57.008279

R. J. Reeder (Ed.) (1983). *Carbonates: Mineralogy and chemistry*.

Rividi, N., van Zuilen, M., Philippot, P., Ménez, B., Godard, G., & Poidatz, E. (2010). Calibration of carbonate composition using micro-Raman analysis: Application to planetary surface exploration. *Astrobiology*, *10*(3), 293–309. https://doi.org/10.1089/ast.2009.0388

Royer, C., Poulet, F., Wiens, R. C., Beck, P., Beyssac, O., Clavé, E., et al. (2024). Mineral composition of Jezero Crater Western fan derived by SuperCam/Mars2020 infrared spectroscopy and spectral modeling. In *LPI contributions* (Vol. 3040, p. 1370). Retrieved from https://ui.adsabs.harvard.edu/abs/2024LPICo3040.1370R

Sanloup, C., Jambon, A., & Gillet, P. (1999). A simple chondritic model of Mars. *Physics of the Earth and Planetary Interiors*, *112*(1–2), 43–54. https://doi.org/10.1016/s0031-9201(98)00175-7

Scheller, E. L., Razzell Hollis, J., Cardarelli, E. L., Steele, A., Beegle, L. W., Bhartia, R., et al. (2022). Aqueous alteration processes in Jezero crater, Mars—Implications for organic geochemistry. *Science*, *378*(6624), 1105–1110. https://doi.org/10.1126/science.abo5204

Swart, P. K. (2015). The geochemistry of carbonate diagenesis: The past, present and future. *Sedimentology*, *62*(5), 1233–1304. https://doi.org/10.1111/sed.12205

Thorpe, M. T., Bristow, T. F., Rampe, E. B., Tosca, N. J., Grotzinger, J. P., Bennett, K. A., et al. (2022). Mars science laboratory CheMin data from the glen Torridon region and the significance of lake-groundwater interactions in interpreting mineralogy and sedimentary history. *Journal of Geophysical Research*, *127*(11), e2021JE007099. https://doi.org/10.1029/2021je007099

Tice, M. M., Hurowitz, J. A., Allwood, A. C., Jones, M. W. M., Orenstein, B. J., Davidoff, S., et al. (2022). Alteration history of Séítah formation rocks inferred by PIXL x-ray fluorescence, x-ray diffraction, and multispectral imaging on Mars. *Science Advances*, *8*(47). https://doi.org/10.1126/sciadv.abp9084

Toppani, A., Robert, F., Libourel, G., de Donato, P., Barres, O., D'Hendecourt, L., & Ghanbaja, J. (2005). A `dry' condensation origin for circumstellar carbonates. *Nature*, *437*(7062), 1121–1124. https://doi.org/10.1038/nature04128

Tutolo, B. M., Hausrath, E. M., Rampe, E. B., Bristow, T. F., Downs, R. T., Kite, E., et al. (2024). In situ evidence for an active carbon cycle on ancient Mars. In *LPI contributions. The woodlands, Texas* (p. 1564).

Urmos, J., Sharma, S. K., & Mackenzie, F. T. (1991). Characterization of some biogenic carbonates with Raman spectroscopy. *American Mineralogist*, *76*, 641–646.

Viviano-Beck, C. E., Seelos, F. P., Murchie, S. L., Kahn, E. G., Seelos, K. D., Taylor, H. W., et al. (2014). Revised CRISM spectral parameters and summary products based on the currently detected mineral diversity on Mars. *Journal of Geophysical Research*, *119*(6), 1403–1431. https://doi.org/10.1002/2014je004627

Wänke, H., & Dreibus, G. (1988). Chemical composition and accretion history of terrestrial planets. *Philosophical Transactions of the Royal Society of London,Series A*.

Wiens, R. C., Maurice, S., Robinson, S. H., Nelson, A. E., Cais, P., Bernardi, P., et al. (2021). The SuperCam instrument suite on the NASA Mars 2020 rover: Body unit and combined system tests. *Space Science Reviews*, *217*(1), 4. https://doi.org/10.1007/s11214-020-00777-5

Yoshizaki, T., & McDonough, W. F. (2020). The composition of Mars. *Geochimica et Cosmochimica Acta*, *273*, 137–162. https://doi.org/10.1016/j.gca.2020.01.011